Aerodynamic Performance Improvement by Divergent Trailing Edge Modification to a Supercritical Airfoil

Neung-Soo Yoo*

Division of Mechanical Engineering and Mechatronics, Kangwon National University, Kangwon-do 200-701, Korea

A computational study has been performed to determine the effects of divergent trailing edge (DTE) modification to a supercritical airfoil in transonic flow field. For this, the computational result with the original DLBA 186 supercritical airfoil was compared to that of the modified DLBA 283. A Navier-Stokes code, Fluent 5. 1, was used with Spalart-Allmaras's one-equation turbulence model. Results in this study showed that the reduction in drag due to the DTE modification is associated with weakened shock and delayed shock appearance. The decrease in drag due to the DTE modification is greater than the increase in base drag. The effect of the recirculating flow region on lift increase was also observed. An airfoil with DTE modification achieved the same lift coefficient at a lower angle of attack while giving a lower drag coefficient. Thus, the lift-to-drag ratio increases in transonic flow conditions compared to the original airfoil. The lift coefficient increases considerably whereas the lift slope increases just a little due to DTE modification.

Key Words : Supercritical Airfoil, Divergent Trailing Edge Modification, Transonic Flow Field, Lift-to-Drag Ratio

Nomenclature

c : Chord
C_d : Drag coefficient
C_l : Lift coefficient
$C_{l\max}$: Maximum lift coefficient
comp : Abbreviation of computation
exp : Abbreviation of experiment
L/D : Lift-to-drag ratio
M : Mach number
p : Pressure
Re : Reynolds number
t : Time
u,v,w : Velocity components in x, y, z directions
V_∞ : Free stream velocity
y^+ : $(\equiv yu_*/\nu)$ Transverse coordinate for the law of the wall
α : Angle of attack
ρ : Density
τ_{ij} : Stress tensor

Superscript
$-$: Average quantity
: Turbulence fluctuation

* Corresponding Author,
E-mail : yoonesoo@kangwon.ac.kr
TEL : +82-33-250-6371; **FAX** : 82-33-257-4190
Division of Mechanical Engineering and Mechatronics, Kangwon National University, Kangwon-do 200-701, Korea. (Manuscript **Received** February 6, 2001; **Revised** July 12, 2001)

1. Introduction

Supercritical airfoils first developed by Whitcomb were designed to weaken and move shock rearward. Supercritical airfoils have a rooftop pressure distribution which implies nearly parallel upper and lower surfaces near the trailing edge. If the trailing edge is sharp, then the geometry is thin in this highly loaded aft region, so blunt trailing edges are often preferred in practice despite its increased base drag.

Henne and Gregg designed divergent trailing edge (DTE) airfoils to reduce drag on blunt supercritical airfoils at high subsonic Mach numbers (Henne and Gregg, 1991). They started

with an existing supercritical airfoil, DLBA (Douglas Long Beach Airfoil) 186, and created a new DTE airfoil, DLBA 243, by varying the airfoil thickness over the aft 10% of chord such that suction and pressure side flows diverge from each other at the trailing edge as shown in Fig. 1. This DTE modification to a blunt supercritical airfoil increases the recirculation zone size in the wake (Lotz, 1995) ; increases the lift-to-drag ratio ; and improves airfoil performance. Until the early 1990s', the transonic aerodynamics of DTE airfoils were calculated (Henne, 1990) by solving both Euler and integral boundary layer equations together using the viscous-inviscid interaction procedure. The use of boundary layer equation forces two approximations. First, the shape of the recirculation in the wake must be specified empirically by locating the streamline that divides forward and reverse flows in the wake. Second, an experimental correlation must be used to estimate the base drag since the code cannot calculate any variables in this region. Henne correlated the calculated results with experimental data at cruise conditions. But, since the flow immediately aft of the trailing edge was guessed, the relationship between the recirculation region and lift-to-drag ratio remains uncertain.

Previous research on divergent trailing edge airfoils did not consider the recirculating flow in the wake, despite the well-established upstream influence of merging suction side and pressure side wake flows on the surface pressure near the trailing edge (Thompson and Whitelaw, 1989). Measurements in the small recirculation region downstream of the blunt divergent trailing edge

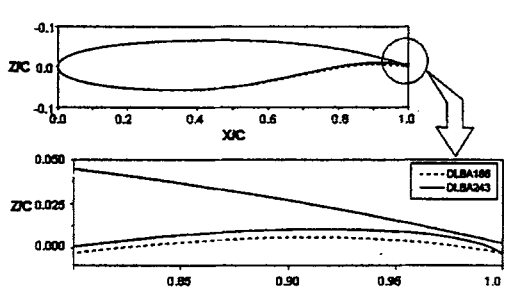

Fig. 1 Geometry of DLBA 186 and DLBA 243 airfoils

are extremely difficult and expensive. Measurements in this region have not been reported to date, probably because its cross stream and streamwise dimensions are about between 0.5% and 2% of chord.

The approach applied in this paper used a validated Navier-Stokes CFD solver, Fluent 5.1, to investigate the relationship between the recirculating flow in wakes and drag reduction associated with DTE modification. Reynolds-Averaged Navier-Stokes equation was solved to accurately represent trailing-edge recirculation regions and shock wave phenomena.

2. Computational Method

The following two-dimensional unsteady compressible Reynolds-Averaged Navier-Stokes equation and the continuity equation were solved.

Continuity Equation

$$\frac{\partial \bar{\rho}}{\partial t}+\frac{\partial}{\partial x}(\overline{\rho u})+\frac{\partial}{\partial y}(\overline{\rho v})=0$$

Momentum Equation

$$\frac{\partial}{\partial t}(\overline{\rho u})+\nabla\cdot(\overline{\rho u V_\infty})=-\frac{\partial \bar{p}}{\partial x}+\frac{\partial \bar{\tau}_{xx}}{\partial x}+\frac{\partial \bar{\tau}_{yx}}{\partial y}$$
$$+\frac{\partial}{\partial x}(-\overline{\rho u' u'})+\frac{\partial}{\partial y}(-\overline{\rho u' v'})$$
$$\frac{\partial}{\partial t}(\overline{\rho v})+\nabla\cdot(\overline{\rho v V_\infty})=-\frac{\partial \bar{p}}{\partial y}+\frac{\partial \bar{\tau}_{xy}}{\partial x}+\frac{\partial \bar{\tau}_{yy}}{\partial y}$$
$$+\frac{\partial}{\partial x}(-\overline{\rho v' u'})+\frac{\partial}{\partial y}(-\overline{\rho v' v'})$$

As a CFD solver, Fluent 5.1 code was used. Fluent 5.1 code utilizes structured/unstructured adaptive mesh Finite Volume Method (FVM). In this study, it was assumed that the flow over the airfoil surface is completely turbulent, and Spalart-Allmaras's one-equation turbulence model was applied. This turbulence model is known as a robust, economical and reasonably accurate method for airfoil flow analysis (Jiang et al., 1997; Strelets et al., 1997). Shock capturing method was used to determine the shock location. This approach is advantageous when the exact shock location is unknown. An explicit time marching method to steady state is employed in this solver. For treating the derivatives, a second

order upwind discretization was adopted.

The grid was constructed using the Gambit pre-processor. All of the computations were done with a 240×100 C-grid as shown in Figs. 2(a) and (b). This grid dimension was obtained by the so-called grid dependence and convergence study (Roache, 1998).

The top and bottom far-field boundaries are located 20 c lengths from the airfoil surface. The upstream and downstream boundaries are also located 20 c lengths away. This spacing was deemed to be sufficient to apply free-stream conditions on the outer boundaries. This was verified for this Navier-Stokes computations by varying the far-field boundary locations. Computational points were clustered near the airfoil surface, including the trailing edge. An adaptive grid was adopted from time to time whenever necessary. The first point above the surface is located at 0.0008 c from the airfoil surface, which corresponds to $y^+ \approx 60$. This type of grid allows the modeling of various airfoils (Yoo, 2000).

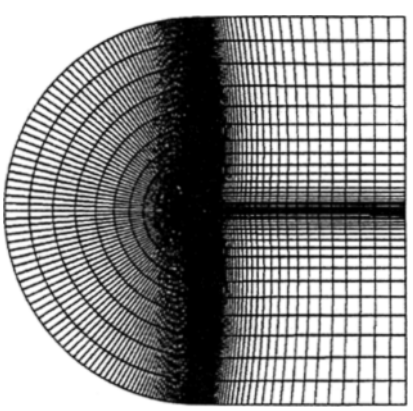

Fig. 2(a) C-Grid system

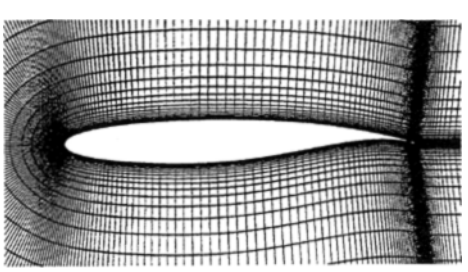

Fig. 2(b) Grid closed-up for DLBA 243 airfoil

3. Results

The CFD procedure adopted in this study needed to be validated. In this study, two benchmark calculations were done, i.e., one for the RAE (Royal Aeronautical Establishment) 2822 airfoil and the other for the DLBA 243 airfoil. These computations were performed within the reported experimental uncertainty of Mach number and angle of attack described in the corresponding figures. The maximum uncertainties in the measured values of angle of attack and Mach number were reported to be about 0.5 degrees and 0.02, respectively, which are consistent with transonic wind tunnel measurements (Henne and Gregg, 1991). Calculations were judged to be converged when the change in lift coefficient per time step was less than 10^{-5}, and typically required about 1,000 time steps. For

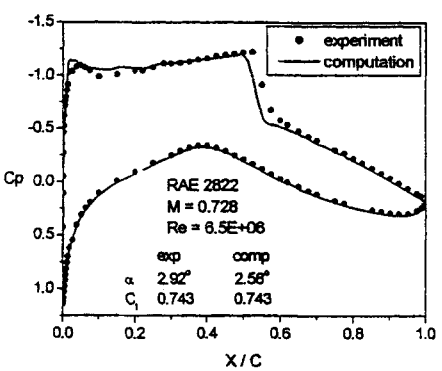

Fig. 3 Measured and computed pressure distributions on RAE 2822 airfoil

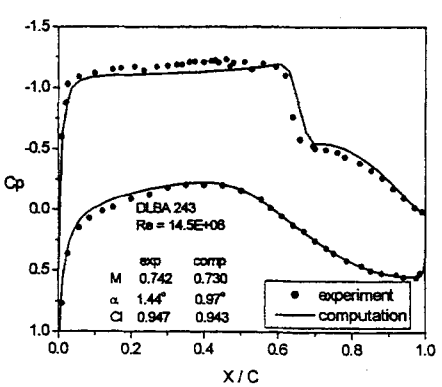

Fig. 4 Measured and computed pressure distributions on DLBA 243 airfoil

selected calculations, iteration was continued to 1, 200 time steps.

Transonic flow around an RAE 2822 airfoil exhibits boundary layer and shock characteristics similar to those on DTE airfoils. The 1980~1981 Stanford Conference (Kline et al., 1980) assessed an RAE 2822 experiment, and, by subsequent recommendations, it was chosen to validate the CFD procedure. Calculated and measured values of the pressure coefficient on airfoil surfaces are in excellent agreement as shown in Fig. 3. All of the parameter values are inscribed in this figure. In this calculation, the difference in the angle of attack is within the uncertainty.

Figure 4 shows another benchmark calculation result, pressure distributions based on the experimental and computational data for DLBA 243 airfoil. The best match between the calculation and the experimental data is obtained for a 0. 97 degree angle of attack at Mach number of 0.73. In this case, the calculated and experimentally measured values of pressure coefficient also agree with each other. Thus, the present computational methods were judged to be satisfactory. Computations were performed for DLBA 186 and DLBA 243 airfoils with the same trailing edge thickness of 0.57% of chord. Computed pressure distributions are presented to provide insight into the flow structures that result in drag reduction. Figures 5 and 6 show the surface pressure distributions over DLBA 186 and DLBA 243 airfoils.

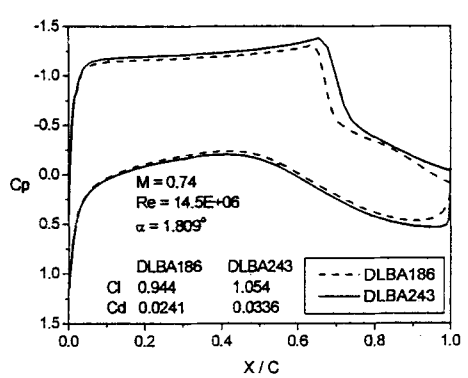

Fig. 5 Pressure distributions on DLBA 186 and DLBA 243 airfoils I

The comparison in Fig. 5 was made at the same angle of attack, Mach number and Reynolds number. The DTE airfoil produced more lift than seed airfoil. The comparison in Fig. 6 was made at the same lift coefficient 0.8, Mach number and Reynolds number. According to the Henne and

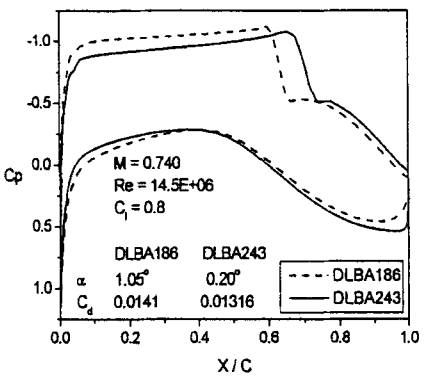

Fig. 6 Pressure distributions on DLBA 186 and DLBA 243 airfoils II

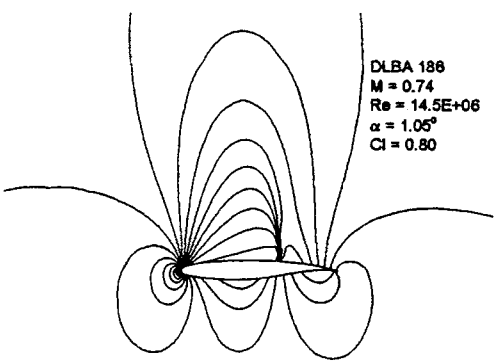

Fig. 7(a) Pressure contours around DLBA 186 airfoil

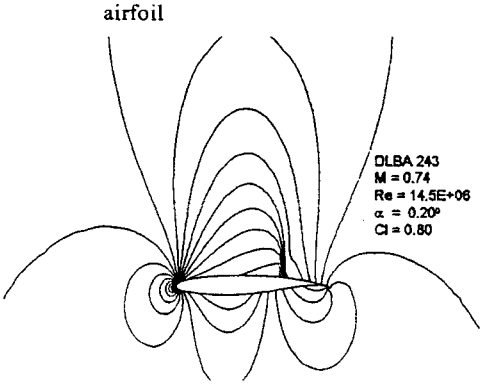

Fig. 7(b) Pressure contours around DLBA 243 airfoil

Gregg's study, the lift coefficient of 0.8 is the design lift coefficient of DLBA 243 airfoil. This comparison is important since lift and drag are the main design parameters. These forces are extremely sensitive to small changes in the angle of attack and Mach number. Figure 6 shows the reduction in shock strength and the delay of shock on the DTE airfoil. Also the lift-to-drag ratio of DTE airfoil is greater than that of seed airfoil.

Figure 7(a) and (b) show the pressure contours around DLBA 186 and DLBA 243 airfoils at the same lift coefficient of 0.8. The DTE airfoil has a weaker, delayed shock compared to the seed airfoil. Figure 8(a) and (b) show velocity vectors in the wake region. The recirculation region consists of a clockwise vortex situated on the upper surface and a more elongated counterclockwise vortex on the pressure side. The recirculation region of the DLBA 243 DTE airfoil is greater than that of the DLBA 186 airfoil. This trailing edge recirculation acts like a chord extension which increases lift.

The effect of angle of attack on the lift coefficient for both airfoils can be seen in Fig. 9.

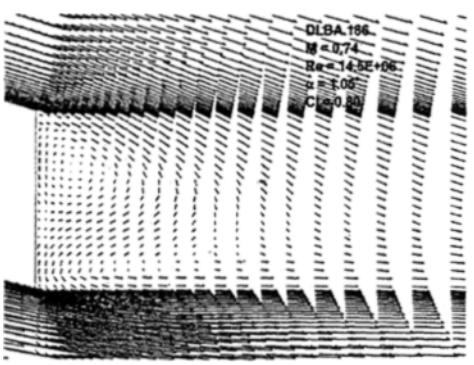

Fig. 8(a) Velocity field behind the trailing edge of DLBA 186 airfoil

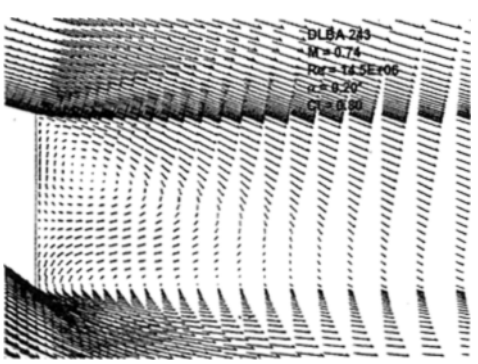

Fig. 8(b) Velocity field behind the trailing edge of DLBA 243 airfoil

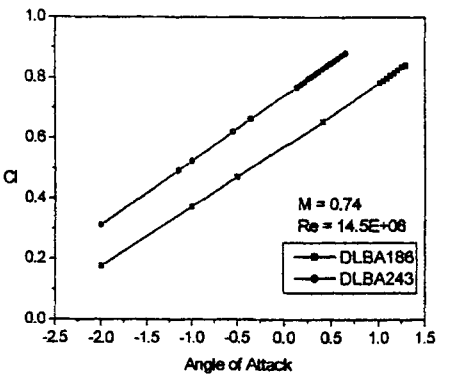

Fig. 9 Lift coefficient versus angle of attack for DLBA 186 and DLBA 243 airfoils

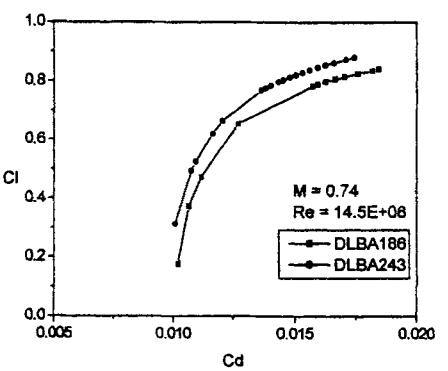

Fig. 10 Drag polars for DLBA 186 and DLBA 243 airfoils

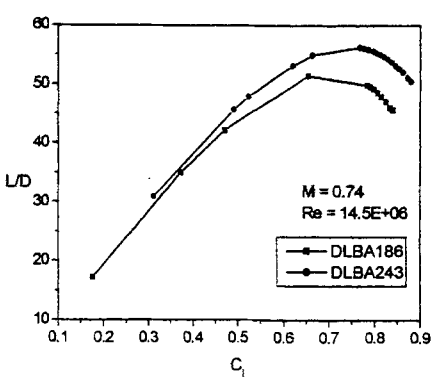

Fig. 11 Lift-to-drag ratio versus lift coefficient

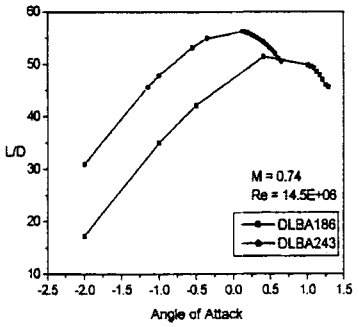

Fig. 12 Lift-to-drag ratio versus angle of attack

The lift coefficient slope as well as the lift coefficient increase due to the DTE modification, although the increase in lift coefficient slope is very small. Figure 10 shows a comparison of the drag polars between DLBA 186 and DLBA 243 airfoils. The lift-to-drag ratio of DLBA 243 is bigger than that of DLBA 186. Figure 11 shows how the lift-to-drag ratio of both airfoils varies as the lift coefficient increases. It is remarkable that, at higher lift coefficients, the difference in L/D between two airfoils increases. The optimum

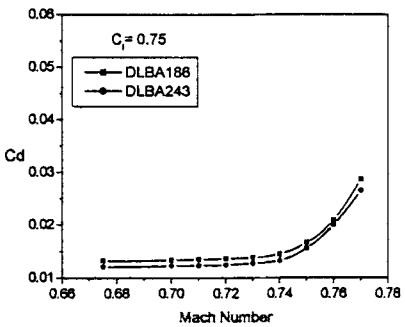

Fig. 13(a) Drag coefficients versus Mach number at a constant lift coefficient of 0.75

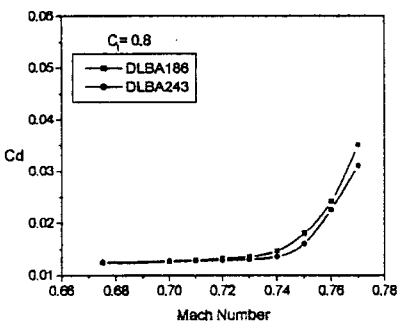

Fig. 13(b) Drag coefficients versus Mach number at a constant lift coefficient of 0.8

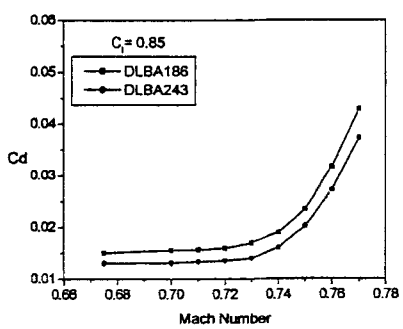

Fig. 13(c) Drag coefficients versus Mach number at a constant lift coefficient of 0.85

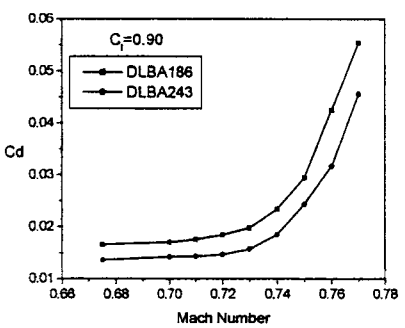

Fig. 13(d) Drag coefficients versus Mach number at a constant lift coefficient of 0.9

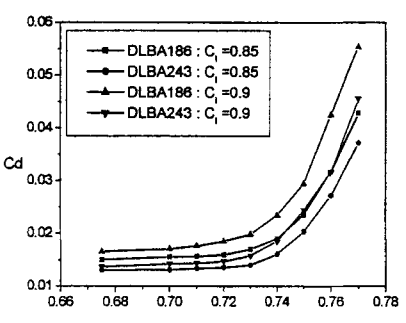

Fig. 13(e) Drag coefficients versus Mach number at a constant lift coefficients of 0.85 and 0.9

lift coefficient for Mach number of 0.74 can be estimated. The relation between the lift-to-drag ratio and the angle of attack for two airfoils can be seen in Fig. 12. The DTE modification is not always superior to the seed airfoil. The aerodynamic efficiency of DLBA 243 DTE airfoil is superior to the original DLBA 186 airfoil in every respect, (i. e., L/D, $C_{l\max}$, etc), if the angle of attack is not bigger than about 0.6 degrees.

Drag characteristics as functions of Mach number at a given lift coefficient for both airfoils are presented in Figs. 13(a), (b), (c), (d), and (e). In every case, the drag coefficients of DTE airfoil are less than that of the seed airfoil. In Fig. 13(e), it is found that the C_d of DLBA 243 at C_l=0.9 is even less than that of DLBA 186 at C_l=0.85 over the wide range of Mach number.

Finally, Figs. 14(a) and (b) represent lift-to-drag ratio as a function of Mach number. From these results, C_l=0.8 is reasonably chosen as the design lift coefficient for the DLBA 186 airfoil. But, for the DLBA 243 DTE airfoil, it is difficult to choose the design value of C_l as seen in Fig. 14 (b). Also the sensitivity of L/D to C_l at all Mach numbers is greater for DLBA 186 than DLBA 243.

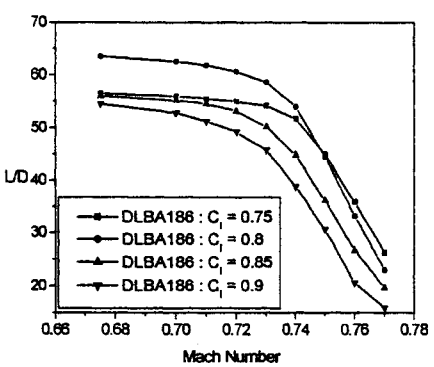

Fig. 14(a) Lift-to-drag ratio versus Mach number for DLBA 186

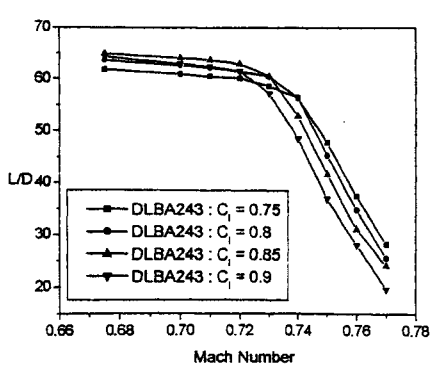

Fig. 14(b) Lift-to-drag ratio versus Mach number for DLBA 243

4. Conclusions

A computational study has been performed to investigate the effect of divergent trailing edge (DTE) modification to the original supercritical airfoil DLBA 186. Fluent 5.1, a Navier-Stokes code, was used with Spalart-Allmaras's one -equation turbulence model. From the comparison of computational results for DLBA 243 DTE airfoil and DLBA 186 airfoils, the following conclusions were drawn :

(1) At the same lift coefficient, drag coefficient can be reduced at all test speeds on supercritical airfoils by DTE modification. This means an improvement in the lift-to-drag ratio. At higher lift coefficients, difference in L/D between two airfoils increases.

(2) Reduction in drag is due to a decrease in the shock-induced drag, resulting from a delayed and weakened shock, which is greater than the increase in base drag.

(3) The pressure difference between the pressure and suction sides of DTE airfoils is more constant from the suction-side shock aft to the trailing edge than that of the seed airfoil.

(4) DTE modification also increases the size of the recirculation region downstream of its blunt trailing edge, increasing lift.

(5) Lift coefficient increases considerably due to the DTE modification and, lift coefficient's slope increase just a little due to DTE modification

(6) DTE modification improves aerodynamic performance in every aerodynamic respect, maximum lift coefficient, lift slope, lift-to-drag ratio, maximum lift-to-drag ratio, etc.

However, above conclusions have some limitations. They are valid for lift coefficient values near the design lift coefficient and

transonic Mach numbers.

References

Henne, P. A., 1990, "Innovation with Computational Aerodynamics : The Divergent Trailing Edge Airfoil," *Applied Computational Aerodynamics*, edited by P. A. Henne, AIAA Inc., Washington, D. C., pp. 221~261.

Henne, P. A., and Gregg, R. D., 1991, "New Airfoil Design Concept," *Journal of Aircraft*, Vol. 28, No. 5, pp. 300~311.

Jiang, Y. T., Damodaran, M. and Lee, K. H., 1997, "High-Resolution Finite Volume Computation of Turbulent Transonic Flow past Airfoils," *AIAA J*, Vol. 35, No. 7, pp. 1134~1142.

Kline, S. J., Cantwell, B. J., and Lilley, G. M. Editors, 1980, "1980-81 *AFOSR HTTM Stanford Conference on Complex Turbulent Flows*: Comparison of Computation and Experiments," Thermosciences Division, Mechanical Engineering Dept., Stanford University, Stanford, California.

Lotz, R. D., 1995, "Grid Dependence and Numerical Uncertainty Analysis of a Transonic Airfoil Calculation," *MS Degree Thesis*, R.P.I., New York.

Roache, P. J., 1998, "Verification of Codes and Calculations," *AIAA Journal*, Vol. 36, No. 5, pp. 696~702.

Strelets, M. Kh., Travin, A. K. and Shur, M. L., 1997, "A Computation between One and Two -Equation Differential Models of Turbulence in Application to Separated and Attached Flows: Transonic Flow Around Airfoil," *High Temperature*, Vol. 35, No. 2, pp. 298~310.

Thompson, B. E., and Whitelaw, J. H., 1989, "Trailing-Edge Region of Airfoils," *Journal of Aircraft*, Vol. 26, No. 3, pp. 225~234.

Yoo, N. S., 2000, "Effect of the Gurney Flap on a NACA 23012 Airfoil," *KSME International Journal*, Vol. 14, No. 9, pp. 1013~1019.